IEEE Access
Multidisciplinary ⋮ Rapid Review ⋮ Open Access Journal

Received August 17, 2020, accepted August 27, 2020, date of publication September 1, 2020, date of current version September 16, 2020.

Digital Object Identifier 10.1109/ACCESS.2020.3021034

Evaluating Multivariable Statistical Methods for Downscaling Nighttime Land Surface Temperature in Urban Areas

PENGCHENG QI[1,2], YAN CUI[1], HAIJUN ZHANG[1], SHIXIONG HU[3], LUNGUANG YAO[1], AND LARRY BAILIAN LI[4,5]

[1]Collaborative Innovation Center of Water Security for Water Source Region of Mid-Line of South-to-North Diversion Project of Henan Province, Nanyang Normal University, Nanyang 473061, China
[2]College of Environment and Planning, Henan University, Kaifeng 475004, China
[3]Department of History and Geography, East Stroudsburg University of Pennsylvania, East Stroudsburg, PA 18301, USA
[4]Ecological Complexity and Modeling Laboratory, Department of Botany and Plant Sciences, University of California–Riverside, Riverside, CA 92521, USA
[5]International Joint Laboratory of Watershed Ecological Security and Collaborative Innovation Center of Water Security for Water Source Region of Middle Route Project of South-North Water Diversion in Henan Province, College of Agricultural Engineering, Nanyang Normal University, Nanyang 473061, China

Corresponding author: Pengcheng Qi (qipengchengsd@163.com)

This work was supported in part by the National Natural Science Foundation of China under Grant 41201099 and Grant 51879130, in part by the University Youth Excellent Teacher Training Program of Henan Province under Grant 2016GGJS-126, in part by the Scientific Research and Service Platform fund of Henan Province under Grant 2016151, in part by the fund of Scientific and Technological Innovation Team of Water Ecological Security for Water Source Region of Mid-line of South-to-North Diversion Project of Henan Province, and in part by the Postdoctoral Research Funds of Henan University under Grant BH2012042.

ABSTRACT For research and practice in fields such as the environment and meteorology, nighttime land surface temperature (LST) images at fine resolution provide important basic data. Since only a few satellite sensors can take fine-resolution thermal infrared images at night, such images are rather scarce. Downscaling of coarse-resolution LST images is a potential method for obtaining high-resolution LST images. However, downscaling methods have been mostly proposed for daytime LST images. This study aimed to evaluate the performance of methods that combine multiple explanatory variables and machine learning algorithms for downscaling coarse-resolution nighttime LST images in urban areas. Verification showed that the errors in the downscaling results were acceptable (mean absolute errors within 2 K). The resulting images could depict the spatial pattern of night LST in the study area in great detail. It was demonstrated that visible-near infrared images taken in the daytime could be used for downscaling of nighttime LST images, the rationality of which was deduced. It was also demonstrated that the performance of the spectral explanatory variables in nighttime LST downscaling was not lower than that of the mechanism explanatory variables. This method has high application value in many academic and practical efforts, such as land-atmosphere interface radiation budget studies, suitability assessments of human settlement, and urban environmental planning.

INDEX TERMS Advanced spaceborne thermal emission and reflection radiometer (ASTER), downscaling, land surface temperature (LST), landsat 8 operational land imager (OLI), moderate resolution imaging spectroradiometer (MODIS), nighttime, urban areas.

I. INTRODUCTION

Land surface temperature (LST) reflects the intensity of molecular thermodynamic movements of surface substances and the thermal degree of the land surface [1], [2]. LST has a profound impact on the intensity of energy flow and exchange of substances between the earth and atmosphere. Numerous studies on urban thermal environmental monitoring [3]–[5], land surface processes [6]–[8], estimations of soil moisture [9]–[11] and evapotranspiration [12]–[14] and other related aspects based on LST data from thermal infrared remote sensing have been reported. Most of the existing research is based on LST data obtained during daytime. However, the research and application values of nighttime LST data are as important as those of daytime LST data. In the environment, nighttime LST directly influences the thermal

The associate editor coordinating the review of this manuscript and approving it for publication was Qingli Li.

comfort of the environment and thus affects the intensity of human outdoor activities [15], [16]. Furthermore, this factor can indirectly influence urban weather and atmospheric pollution at night through stability and the thermodynamic properties of the boundary layer as well as the height of the mixed layer. In the fields of forestry and ecology, the nighttime temperature of the canopy or soil has special significance for individual organisms and ecosystems. Therefore, nighttime LST data have important research significance and application values. However, research on regional nighttime LST is limited.

Satellite-borne thermal infrared remote sensing images are the most important data sources for depicting LST at regional scales due to their advantage of providing spatially continuous and simultaneous views of an area [17], [18]. However, most satellite-borne thermal infrared sensors produce images only in the daytime. Although some sensors, such as the Moderate Resolution Imaging Spectroradiometer (MODIS) and Geostationary Operational Environmental Satellite Imager, can take thermal images at night, the spatial resolution of their images is too coarse to be suitable for many applications. The Advanced Spaceborne Thermal Emission and Reflection Radiometer (ASTER) has relatively finer spatial resolution but has a long revisit interval and low probability of acquiring high-quality images due to cloud disturbances. This limitation may explain why there is currently minimal research using nighttime LST data at regional scales.

In the absence of fine-resolution satellite sensors capable of imaging at night, a potential solution is to downscale coarse-resolution LST images. Until now, numerous studies have been conducted to develop various methods for daytime LST downscaling (in fact, the downscaling objects in previous studies have included three types: digital number (DN) images in the thermal infrared band, brightness temperature images, land surface temperature images; for simplicity, we refer to these as LST in this section). These methods are also called LST image sharpening, subpixel temperature estimation or disaggregation of LST in previous literature. These methods can be categorized into three groups [19]: statistical [18], [19], physical [20], [21] and spatiotemporal methods [22]–[24]. Among these groups, statistical methods have received more attention due to their accuracy and simplicity [1], [19]. The conceptual framework of statistical LST downscaling methods involves the following steps: (1) construct an LST model (i.e., a statistical relationship between LST and explanatory variables) using sample pixels from coarse-resolution images of these variables and (2) simulate LST at fine resolution by inputting fine-resolution images of the explanatory variables into the LST model. The two following paragraphs provide an analysis of previous studies from the aspects of explanatory variables and regression tools, respectively.

One trend of statistical LST downscaling research is the increase in the number of explanatory variables. Most early methods used a single explanatory variable, such as the normalized difference vegetation index (NDVI) [18], [25]–[27]. However, although those methods are effective in homogeneous agricultural areas, they may not perform well in highly heterogeneous areas, such as urban areas. To improve the robustness and accuracy of LST downscaling methods, many recent studies have used multiple explanatory variables. We call these methods multivariable statistical methods. They can be further divided into the following three categories: (1) directly using raw DN or reflectivity of the visible-near infrared (VNIR) bands as explanatory variables [28], [29], which we call spectral explanatory variables; (2) transforming those VNIR images to derive remote sensing indexes and then using these as the explanatory variables [30]–[34], which theoretically has more specific physical meaning than the previous images; we call these mechanism explanatory variables; (3) adding auxiliary data, such as meteorological data and digital terrain models on the basis of the previous categories [35], [36]. The literature that has used the first category of explanatory variables has emphasized the benefits of doing so, namely, simplifying the processing steps on the premise of accurate downscaling results. In contrast, the literature that has used the second category considered that these variables were more conducive to LST downscaling because they had more significant biophysical implications of surface energy balance (SEB). When the research area was large or mountainous, use of the third category of explanatory variables could significantly improve the accuracy of LST downscaling methods [35].

Given the increased numbers of explanatory variables used in LST downscaling, simple regression tools are not competent to determine the statistical relationship between LST and explanatory variables. At present, machine learning algorithm are used to solve this problem. In [30], a genetic algorithm and self-organizing feature map artificial neural network (ANN) were utilized to model the relationships between LST and 4-9 land-surface parameters. Gao *et al.* [28] employed a regression tree algorithm to train the relationship between brightness temperature and top-of-atmosphere reflectance for six VNIR bands and found that the algorithm could avoid the risk of overfitting and reduce the sensitivity of downscaling results to errors in the input variables. In [19], machine learning algorithms (i.e., random forest regression (RFR), support vector regression (SVR), and extreme learning machine (ELM)) outperformed a traditional temperature sharpening technique (TsHARP), and ELM performed better than RFR and SVR. In [29], machine learning algorithms (i.e., gradient boosting machine and support vector machine) solved the problem of large numbers of explanatory variables and strong collinearity between them so they could competently distinguish the most important explanatory variables from more than 100 candidate variables (hyperspectral bands) and then accurately simulate fine-resolution LST. In contrast, Wang *et al.* [34] pointed out that the machine learning method was not always superior to simple linear regression in terms of simulation accuracy and that a two-variable interaction model would be sufficient to downscale the daytime or nighttime LST images.

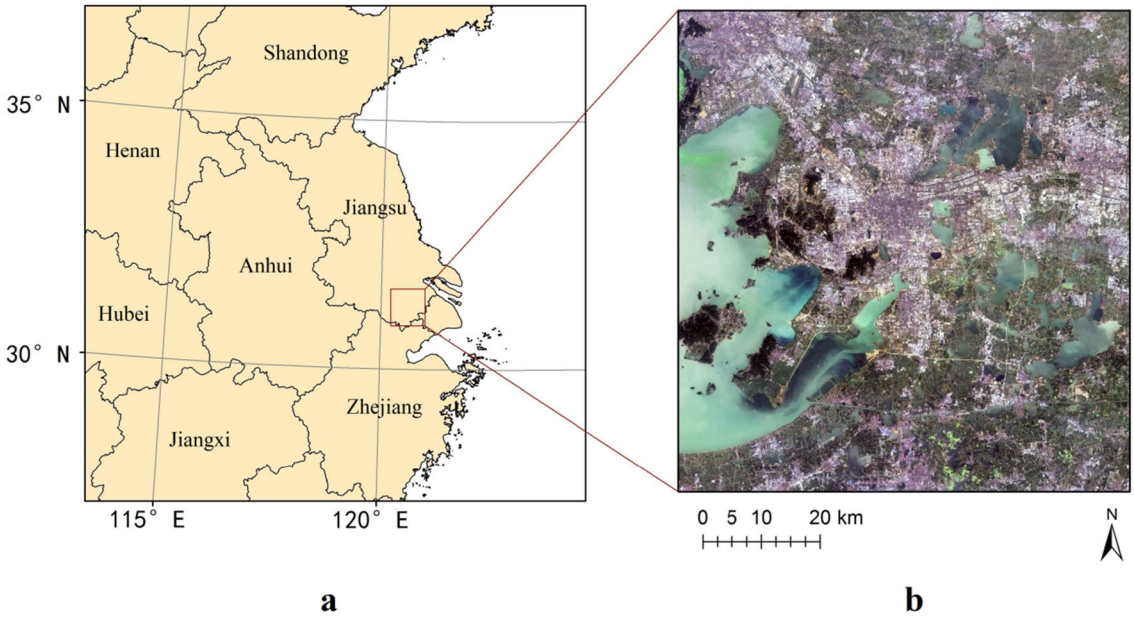

FIGURE 1. The study area. (a) The location of the area; (b) The area shown using a true color composite image from Landsat 8 OLI.

Thus far, most LST downscaling methods were developed for daytime LST, while only a few were developed for nighttime LST, such as [37]. Nichol classified a SPOT-5 image to derive a land cover type image and then used the latter to generate an emissivity image; finally, based on the emissivity image, a nighttime brightness temperature image was corrected to an LST image while enhancing its spatial resolution [37]. The reliability of that method depends on the influence of emissivity on the nighttime LST as well as the accuracy of the emissivities estimated based on land cover types.

As a state variable in the complicated process of SEB, the spatial variability of nighttime LST depends on spatial variations of the energy budget in a certain time range before the time being studied, so it also depends on the spatial variations of various environmental factors in these processes. Emissivity, the unique explanatory variable in [37], is only one of these factors. Therefore, in theory, using a multivariable method is better than using a single variable method to improve the accuracy of nighttime LST downscaling. However, how to accurately depict the spatial distributions of these environmental factors at night becomes a question worthy of deliberate consideration. Specifically, only daytime VNIR images are potential data to depict the nighttime environmental factors because VNIR images cannot be obtained from satellite-borne sensors at night. The rationality and reliability of using VNIR images taken in the daytime for downscaling of nighttime LST image need to be discussed and verified.

This study aimed to evaluate the performance of the multivariable statistical methods for downscaling nighttime LST. Specifically, the object of downscaling was the 1000-m resolution nighttime MODIS LST product; the explanatory variables were calculated from Landsat 8 Operational Land Imager (OLI) and Thermal Infrared Sensor (TIRS) images, which were obtained during the daytime; the ASTER nighttime LST product was used as the validation set. Since MODIS LST products, Landsat data, and similar data are easy obtainable by ordinary users worldwide, if this method is shown to be reliable, this method will be of great significance for many academic and practical works. There are two key issues in this framework: (1) Can daytime VNIR images be used for downscaling nighttime LST? (2) Which of the spectral explanatory variables or mechanism explanatory variables is more suitable for LST downscaling? For these two questions, based on the verification of the downscaling results of this study, the answers were obtained and the reasons were analyzed in this paper.

II. MATERIALS AND METHODS

A. STUDY AREA

The study area is a rectangular area beginning at longitude 120.23°E, latitude 30.87°N to longitude 121.03°E, latitude 31.61°N. It is located in the southeast of Jiangsu Province (Figure 1), covering municipal districts of Suzhou and the surrounding areas thereof. The area was selected as study area given its diversity of land cover types and availability of various types of data. The main land use and cover types are urban land, forestland, cultivated land, and water body. In particular, urban land has a complex composition, including industrial areas, commercial areas, residential areas, and areas under construction.

B. DATA SOURCE AND PREPROCESSING

Figure 2 shows the workflow of the present study.

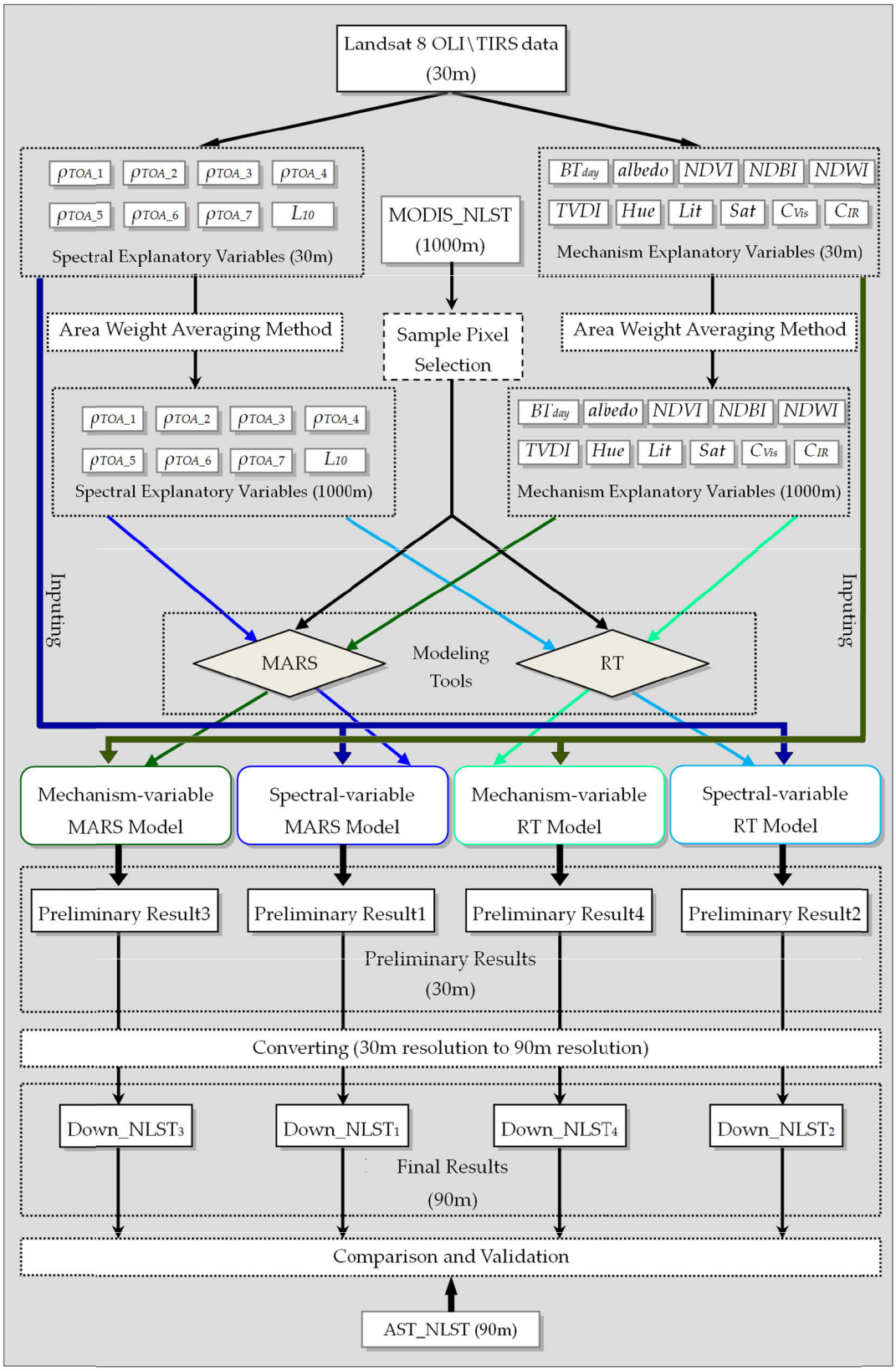

FIGURE 2. A schematic workflow of the current study.

In this study, MODIS was used to provide a coarse resolution nighttime LST image. Although both Terra MODIS and Aqua MODIS could take images at night, considering that this study was a methodology study, we selected the former for testing. The Terra MODIS data were downloaded from the National Aeronautics and Space Administration (NASA) Distributed Active Archive Center (DAAC) located in the Goddard Space Flight Center in Greenbelt, Maryland. The image was a level-3 data product (MOD11A1, Collection-5) in HDF format, and the original image was taken by Terra MODIS at 14:13:41 UTC on October 1st, 2015 at H28V05. The Collection-5 was the latest version available when we downloaded the data. The HDF file was decompressed to extract the nighttime LST image (denoted as MODIS_NLST) and data quality control marks (QA) and then projected into an image at 1000-m resolution in the WGS84 Universal Transverse Mercator (UTM) coordinate system. Based on the QA, the pixels with an error greater than 2 K in the MODIS_NLST image were removed.

Landsat 8 OLI\TIRS data were obtained from EarthExplorer of the United States Geological Survey (USGS). They were geometrically fine-calibrated images (in UTM coordinate system) taken at 2:31:11 UTC on October 13th, 2015 with a WRS-2 path\row number of P119R38. Except the panchromatic wave band, all the remaining bands of Landsat 8 OLI\TIRS were at 30-m resolution.

The ASTER nighttime LST image (denoted as ASTER_NLST) was used to conduct a cross-comparison. This type of data had been used in several previous similar studies [30], [38], [39], and the reliability meets the requirements of the study. The image was obtained from USGS EarthExplorer and was a level-2 data product (AST08) in the UTM coordinate system, and the original image was taken by Terra ASTER sensor at 14:13:41 UTC on October 1st, 2015.

A 12-day difference is noted between OLI\TIRS data and MODIS\ASTER data. In practical applications, there are usually time differences of days or even dozens of days between coarse-resolution LST images and fine-resolution explanatory variable images. The 12-day difference in this study reflects the reality.

C. SELECTION OF EXPLANATORY VARIABLES AND GENERATION OF THEIR RASTER LAYERS

In the current study, two groups of explanatory variables were used to construct nighttime LST model (i.e., statistical relationship between nighttime LST and explanatory variables). One group was spectral explanatory variables, which were mainly expressed in the apparent reflectance images of VNIR bands. The other group was mechanism explanatory variables, which were chosen mainly based on the previous studies focusing on SEB [40]–[43] and expressed in raster layers gained from calculation or transformation of VNIR DN images; each of these variables pointed to a specific environmental factor that might affect nighttime LST in the process of surface energy budget. The nighttime LST model that was constructed by the first group of explanatory variables was purely statistical, whereas the LST modeling based on the second group of explanatory variables was performed to integrate human being's knowledge on land SEB processes into the statistical model. The goal of this experimental design was to observe whether the LST models based the two explanatory variable groups exhibit significant differences in accuracy.

1) SPECTRAL EXPLANATORY VARIABLES

This group has 8 variables, including the apparent reflectivity of Landsat 8 OLI bands 1-7 (recorded as ρ_{TOA_i}, $i = 1$ to 7) and the atmosphere top radiance of Landsat 8 TIRS band 10 (recorded as L_{10}). The ρ_{TOA_i} was calculated as follows [44]:

$$\rho_{TOA\_i} = \left(M_i Q_{cal\_i} + A_i\right) / \cos\theta_z \quad i = 1 \text{ to } 7 \tag{1}$$

where Q_{cal_i} are the Level 1 DN value, and M_i and A_i, which are acquired from the header file, are the reflectivity multiplicative rescaling factor and the reflectivity additive rescaling factor of the band i, respectively. Here, θ_z is the solar zenith angle of the study area at the imaging moment.

The formula to calculate the atmosphere top radiance of the thermal infrared band (L_{10}) is noted as follows [44]:

$$L_{10} = M_{10} Q_{cal\_10} + A_{10} \tag{2}$$

where M_{10} and A_{10} are the radiance multiplicative rescaling factor and the radiance additive rescaling factor of band 10, respectively, which are acquired from the header file.

2) MECHANISM EXPLANATORY VARIABLES

Numerous factors can influence LST, such as net shortwave radiation, air temperature, wind speed as well as moisture, specific heat capacity, thermal conductivity and density of the land surface. However, abundant exogenous data (e.g., digital terrain model and meteorological data) must be introduced to simulate distribution of all abovementioned factors. One of the purposes of this study was to observe ''whether explanatory variable layers formed by combination and transformation of original optical images based on knowledge only without adding any exogenous data can improve prediction accuracy of nighttime LST''. Thus, a total of 11 variables were selected according to two principles: (1) no exogenous data need to be added during the construction of the variable raster layers; (2) the variables could represent abovementioned environmental factors to a large extent. Specific reasons for selecting them and the methods of generating their raster layers are introduced as follows:

- Daytime LST can be viewed as the basis of nighttime LST. The LST changes occurring from day to night were mainly determined by the characteristics of the land surface. In this study, the daytime brightness temperature (BT_{day}) was employed to proxy daytime LST. Although the value of brightness temperature is not equal to LST, there is a close correlation between them, and the spatial distribution of brightness temperature can well fit that of LST [45], [46]. BT_{day} (K) was calculated by Landsat 8

TIRS Band10 as follows [44]:

$$BT_{day} = 1321.08 \big/ \ln(774.89 \big/ L_{10} + 1) \quad (3)$$

- The shortwave surface albedo (*albedo*) is the ratio of the shortwave radiant flux reflected to the shortwave radiant flux incident on a surface. It reversely determines the capability of land surface to absorb solar radiation. The remote sensing retrieval of *albedo* essentially calculates the broadband albedo from the reflectivity of several narrow bands. Liang [47] proposed retrieval algorithms of *albedo* for a variety of sensors, including the algorithm for retrieving *albedo* from the atmospheric corrected reflectivity of Landsat TM/ETM+ Bands 1, 3, 4, 5, and 7. Landsat 8 OLI Bands 2, 4, 5, 6, and 7 are bands that are similar to Landsat TM/ETM+ Bands 1, 3, 4, 5, and 7. In addition, Xu [48] further proved the high correlation between the corresponding bands of OLI and TM/ETM+. Therefore, the corresponding bands of OLI were input into Liang's algorithm [47] to calculate *albedo*:

$$\begin{aligned} albedo = {} & 0.356\rho_{AR\_2} + 0.130\rho_{AR\_4} + 0.373\rho_{AR\_5} \\ & + 0.085\rho_{AR\_6} + 0.072\rho_{AR\_7} - 0.0018 \end{aligned} \quad (4)$$

  where $\rho_{AR\_i}(i = 2, 4, 5, 6, 7)$ is the reflectivity of the i^{th} band after atmospheric correction. Based on the COST atmospheric correction algorithm [49], ρ_{AR_i} was calculated as follows:

$$\rho_{AR\_i} = (M_i(Q_{cal} - Q_h) + A_i)/\cos\theta_z \quad (5)$$

  where Q_h is the atmospheric correction value obtained by dark object method.
- The thermal capacity and surface roughness of underlying surface are closely related with vegetation quantity [40]. Normalized difference vegetation index (*NDVI*) was selected to represent the factor of vegetation quantity. The *NDVI* image was derived as follows:

$$NDVI = (\rho_{TOA\_5} - \rho_{TOA\_4})/(\rho_{TOA\_5} + \rho_{TOA\_4}) \quad (6)$$

- The land surface in urban areas is mainly composed of nonevaporation and nonpermeation materials, such as asphalt, concrete, stone, metal, etc. Normalized difference build-up index (*NDBI*) is an effective index for downscaling of LST in urban areas [18], [34]. The *NDBI* image was derived as follows [18]:

$$NDBI = (\rho_{TOA\_6} - \rho_{TOA\_5})/(\rho_{TOA\_6} + \rho_{TOA\_5}) \quad (7)$$

- Water is a common surface feature with high thermal capacity. The normalized difference water index (*NDWI*) is an efficient index to distinguish water and lands [50] and can represent the proportion of water in the mixed pixel. The *NDWI* image was obtained using the following equations [50]:

$$NDWI = (\rho_{TOA\_3} - \rho_{TOA\_6})/(\rho_{TOA\_3} + \rho_{TOA\_6}) \quad (8)$$

- The thermal capacity of soil and vegetation is closely related with moisture content. The temperature vegetation drought index (*TVDI*) is a simple and effective index reflecting soil water supply [51]. The *TVDI* image was obtained using the following equations:

$$TVDI = (BT_{day} - BT_{min})/(BT_{max} - BT_{min}) \quad (9)$$

$$BT_{min} = a_1 * (NDVI) + b_1 \quad (10)$$

$$BT_{max} = a_2 * (NDVI) + b_2 \quad (11)$$

  where $BT_{\min}$ and $BT_{\max}$ are the brightness temperatures at wet and dry edges for a given *NDVI*, respectively. The wet and dry edges are the boundaries of NDVI-LST scatter plot and established by linear regression method(see [51]). The functions of the two edges are shown in Equations (10) and (11), where a_1, b_1, a_2, and b_2 were regression coefficients provided by linear regressions.
- Hue (*Hue*), lightness (*Lit*) and saturation (*Sat*) of true color composite images might represent the difference of urban materials to some extent and therefore exhibit a correlation with thermal properties of the urban land surface. The images generation method was determined as follows: true color synthesis results based on OLI bands 4, 3, and 2 were converted into the HLS space, obtaining *Hue*, *Lit*, and *Sat* images.
- The principal component layers of visible light (C_{Vis}) and the principal component layers of mid/near-infrared spectra (C_{IR}) are expected to proxy the thermal properties of land surface, which are difficult to depict directly or the factors that influence the energy balance with unknown mechanism. We performed principal component transformation based on OLI bands 1∼4 and bands 5∼7 respectively, and chose the two resultant first principal components as C_{Vis} and C_{IR}.

Long-wave radiation emitted from land surface is the main component of SEB at night and largely depends on the emissivity in thermal infrared range. Therefore, in theory, emissivity should be taken as an explanatory variable of the LST downscaling model. However, it is difficult to obtain the emissivity directly by remote sensing. A previous study used land-use type data combined with field measurements to estimate emissivity [37]. However, field-measurement procedures will reduce the simplicity and feasibility of LST downscaling method. Moreover, emissivities of buildings, roads and squares are different, and the emissivities of the various building roofs are also different due to the difference of materials. When using remote sensing images to classify land types, those objects are typically divided into the same type of land, which causes the problem of using a constant to express the different emissivities. These errors will be transmitted to final results. In this study, given the close relationship between emissivity and material type and vegetation quantity, the effect of emissivity on LST is implied in hue, lightness, saturation, and NDVI, and we believed that these variables can largely proxy emissivity.

Thus far, 8 layers of spectral explanatory variables (ρ_{TOA_1}, ρ_{TOA_2}, ρ_{TOA_3}, ρ_{TOA_4}, ρ_{TOA_5}, ρ_{TOA_6}, ρ_{TOA_7}, *and* L_{10}), and 11 layers of mechanism explanatory variables (BT_{day}, *albedo*, *NDVI*, *NDBI*, *NDWI*, *TVDI*, *Hue*, *Lit*, *Sat*, C_{Vis}, and C_{IR}) have been generated. The spatial resolutions of these layers were determined by resolution of the original data, 30 m. Based on these layers, the 1000-m resolution layers were produced by area weight averaging method. Specifically, for each explanatory variable, the mean of its pixels corresponding to the scope of every MODIS_NLST pixel was calculated by the zonal statistics tool of ArcGIS (Version 10.1) [52], which was used as the value of the corresponding pixel of a new 1000-m resolution explanatory variable layer. After this process, eight 1000-m resolution spectral explanatory variable layers and eleven 1000-m resolution mechanism explanatory variable layers were prepared.

D. SELECTION OF SAMPLE PIXELS

The objective of this section was to select appropriate pixels from MODIS_NLST as sample pixels. The values of these pixels and the pixels of explanatory variable layers (1000-m resolution) on the corresponding spatial locations would be used in the next step to establish LST models. The basis for selecting sample pixels is the degree of heterogeneity of explanatory variable pixels (30-m resolution) covered by each 1000-m resolution pixel, which is represented by variation coefficient (CV_x):

$$CV_x = \sigma_x / \mu_x \tag{12}$$

where subscript x represents the explanatory variable, μ_x and σ_x are the mean and the standard deviation of 30-m resolution pixel values of the x explanatory variable within each 1000-m resolution pixel, respectively.

A previous study suggested that the statistical model based on pixel samples with lower heterogeneity was more easily applied to finer-resolution explanatory variables compared to that based on pixel samples with higher heterogeneity [28]. However, if we excessively pursued the homogeneity of 30-m resolution explanatory variable pixels covered by each 1000-m resolution sample pixel (i.e., CV_x was equal to or close to zero), the majority of the selected sample pixels would have belonged to the large homogenous land patches with weak representativeness of fine and broken land patches, and the distribution of sample values would have been more concentrated than that of population values. If the extremely homogenous sample-based model had been applied to the entire study area, large errors would have been generated.

Compromises between heterogeneity and representativeness were made here. Specifically, for each 1000-m resolution pixel, the CV_x was calculated. All the 1000-m resolution pixels were sorted by CV_x from high to low. Then, the top 33% pixels in terms of CV_x were eliminated as more heterogeneous pixels, while the remainder were retained as sample pixels for modeling. Finally, the pixels selected as samples account for 31.5% of the total 1000-m resolution pixels.

E. MODELING METHODS

Above two groups of explanatory variables (8 spectral explanatory variables and 11 mechanism explanatory variables) on sample pixels were separately used as independent variables, while the LST on spatially corresponding sample pixels in MODIS_NLST were used as dependent variables to establish the statistical relationship model between the LST and explanatory variables. Two modeling methods were employed: multivariate adaptive regression splines (MARS) and regression tree (RT).

MARS is an efficient regression modeling method, which can predict an output variable according to multiple independent variables. This method is suitable for finding complex data structures hidden in high-dimensional data. The method divides the high-dimensional feature space into several subspaces. In each subspace, an independent function is employed for fitting. See literature [53] for details.

RT is a type of nonparametric regression applicable to high dimensional data with good effects on nonlinear problems. This method partitions training samples continuously through recursion of the binary branching, and the mode of each branching depends on the "heterogeneity standard", aiming at the maximum decline of the variation of the objective variables in the two sub-nodes. With continuous binary branching, the homogeneity level of the samples in each node increases continuously and finally reaches the highest. The final result in the form of a rule tree obtained after trimming represents the relation between the LST and explanatory variables. See literature [54] for details.

The above two modeling methods and two groups of explanatory variables are crossed to form four models: the spectral-variable-MARS model, spectral-variable-RT model, mechanism-variable-MARS model and mechanism-variable-RT model.

F. SIMULATION OF NIGHTTIME LST IMAGES AND RESULTS VALIDATION

The 30-m resolution explanatory variable raster layers were input into the four models established in the previous section successively by the ArcGIS (Version 10.1) raster calculation tool, yielding four preliminary downscaled nighttime LST images (30 m resolution). Since the spatial resolution of validation image (ASTER_NLST) is 90 m, it is necessary to convert the preliminary downscaled images into the images with 90-m resolution for comparison. The following procedure was performed to convert each preliminary downscaled image as follows: every 3×3 pixels in the preliminary downscaled image is aggregated into one pixel with a resolution of 90 m, and the pixel value was the average value of those 3×3 pixel values. These results were noted as Down_NLST$_1$, Down_NLST$_2$, Down_NLST$_3$, and Down_NLST$_4$ (see Figure 2), which are hereinafter referred to as downscaling results. The mean absolute error (MAE) and root mean square error (RMSE) of the downscaling results were calculated using ASTER_NLST as a reference

TABLE 1. Basic parameters and errors of the downscaling results.

Downscaling Results	Type of Explanatory Variable	Modeling Method	Mean of Result	σ of Result	MAE(K) of Result	RMSE(K) of Result	R^2
Down_NLST$_1$	Spectral	MARS	291.104	2.583	1.475	1.758	0.813
Down_NLST$_2$	Spectral	RT	291.152	2.382	1.476	1.757	0.809
Down_NLST$_3$	Mechanism	MARS	290.722	2.832	1.761	2.198	0.744
Down_NLST$_4$	Mechanism	RT	291.057	2.475	1.547	1.841	0.795

Note: R^2 is the determination coefficients between the downscaling result and validation set.

TABLE 2. The methods and resulting errors of previous similar studies.

Literature	Daytime / Nighttime	Resolution of Source Image (m)	Resolution of Result Image (m)	Method	RMSE (K)	MAE (K)
This Study	Nighttime	1000	90	MARS based on spectral variables	1.758	1.475
Bala et al. [18]	Daytime	1000	100	Bi-square regression based on NDBI	0.97–1.30	N/A
Ebrahimy & Azadbakht [19]	Daytime	960	240	RFR, SVR, and ELM	average 2.5	average 1.74
Kustas et al. [25]	Daytime	1536	192	NDVI-based function	1.61	N/A
Agam et al. [26]	Daytime	960	60	four forms of NDVI-based function	1.18–3.27	N/A
Gao et al. [28]	Daytime	960	120	RT	N/A	0.67
Yang et al. [30]	Daytime	1080	90	ANN	1.57–3.98	N/A
Wang et al. [34]	Daytime and Nighttime	990	30	global regression for urban thermal sharpening using 1–3 explanatory variables.	6.50 (daytime) 3.40 (nighttime)	5.32 (daytime) 2.69 (nighttime)
Wang et al. [38]	Daytime	1000	90	double-step pixel decomposition	2.72	N/A
Jeganathan et al. [55]	Daytime	990	90	resolution-adjusted global model, piecewise regression model, stratified model, and local model	3.24–3.68	N/A
Mukherjee et al. [56]	Daytime	960	120	regression-kriging	0.68	N/A

to measure accuracy. Moreover, the determination coefficients (R^2) of the results with ASTER_NLST were calculated.

III. RESULTS AND ANALYSIS

The errors of the four downscaling results are shown in Table 1. These results were compared with a cubic convolution resampling result of MODIS_NLST (CC_NLST). The reason that we performed the comparison was as follows: The cubic convolution resampling method is a traditional method to obtain finer-resolution image and is easy to operate. Typically, a newly proposed method has application values only when it achieves greater accuracy than cubic convolution resampling method. The MAE, RMSE, and R^2 of CC_NLST are calculated as 1.710 K, 2.0814 K, and 0.707, respectively. Table 1 demonstrates that all results except Down_NLST$_3$ exhibit significantly lower MAE and RMSE than CC_NLST and higher R^2, indicating that the proposed downscaling method is superior to the cubic convolution resampling method.

In Table 1, both MARS modeling and RT modeling methods, the models based on mechanism explanatory variables exhibit higher errors than the models based on spectral explanatory variables. The reasons and practical implications of this phenomenon will be analyzed in Section IV.B.

Several previous studies on surface thermal information downscaling (or known as sharpening or subpixel temperature estimation) are selected for comparison, which resolution is similar or partly similar to this study. Their research methods and resulting errors are described in Table 2. Based on Table 2, it can be inferred that RMSE and MAE of the results obtained in this study are at a moderate level compared to those of the previous studies.

The most significant difference between this study and most previous studies is the difference in downscaling objects. Those studies focused on downscaling of daytime LST, whereas this study focused on downscaling of nighttime LST. In addition to this difference, the following difference also requires attention. Most of the previous studies were methodological studies and assumed an idealized setting for the task scenario. Those studies used a fine-resolution LST image (LST_{fine}) to create a coarse-resolution LST image ($LST_{coarse\_artificial}$) and then used the sample pixels in the $LST_{coarse\_artificial}$ for modeling and then simulating a new fine-resolution LST image (LST'_{fine}). Finally, LST_{fine} was used to verify LST'_{fine}. However, for actual task scenarios,

the LST_{fine} does not exist and is the target of simulation. The present study is an actual-case-based study that used the true images from different sensors (MODIS_NLST and ASTER_NLST) as the modeling samples and the verification data and therefore was affected by several additional factors, such as the geo-referencing accuracy, the date/time difference, and the quality of validation set, leading to larger errors than those of assumed-case-based studies. Thus, the error level of this study as an actual-case-based study is acceptable.

The downscaling results ($Down\_NLST_1$ to $Down\_NLST_4$) of different models and the validation image (ASTER_NLST) are presented (Figure 3a-e). To save space, only locals of the images are shown. The downscaling results and validation image are compared visually for qualitative assessment of the downscaling effect. Compared to validation images (Figure 3e), $Down\_NLST_1$ (Figure 3a), $Down\_NLST_2$ (Figure 3b), and $Down\_NLST_4$ (Figure 3d) exhibit no significant visual errors, while $Down\_NLST_3$ (Figure 3c) exhibits evident errors at some places. Compared to other three downscaling results, the spatial differentiation pattern of nighttime LST reflected by $Down\_NLST_1$ (Figure 3a) exhibits the highest visual similarity with the validation image.

The downscaling results provide sufficient details on the spatial variability of nighttime surface temperature. These images, together with land classification map (Figure 3(f)), enable us to conveniently observe the relationship between the nighttime surface temperature and the land types. Based on visual examination, the downscaling results reflect differentiation patterns of the nighttime surface temperature between land and water accurately, and the distinct water-land boundaries can be observed. The surface temperature of land area is significantly lower than that of water area. This finding confirms to Jensen's [57] diurnal changes of LST of urban objects. That literature showed that the thermal capacities of non-water objects were lower than that of water bodies and the temperature of non-water objects changed quickly and began to be lower than temperature of water after ''thermal crossover''. The term of ''thermal crossover'' in the literature referred to the times when the main objects, such as soil, rock and water, have the same radiant temperature. Usually, the thermal crossovers occur after sunrise and near sunset. The simulation time in this study was 22:14 (local time), which is later than the after-sunrise thermal crossover. Therefore, the land surface temperature at that time was significantly lower than the water surface temperature.

Both the downscaling results and the validation image show that industrial and commercial lands are the land types with the lowest nighttime LST. Further observation of finer-resolution images in Google Earth reveals that such low-temperature land are mainly factories and warehouses. This finding could be explained as follows: most factories and warehouses are roofed by color-steel plates, which have lower heat storage capacity due to thermodynamic properties (e.g., thermal conductivity) compared with roof materials of residential buildings. In addition, the simple and consistent geometric structure of factories and warehouses forms low-roughness surfaces that more easily dissipate heat that accumulates at daytime.

In downscaling results and validation image, forestry and residential lands have close nighttime LST, which is lower than LST on water and higher than LST on industrial and commercial lands. This finding disagrees with research conclusions of Jensen [57], indicating that LST at night in industrial and commercial lands was slightly higher than that in vegetation and agricultural regions. This finding might be related with different roof materials of main commercial and industrial buildings in these two cities.

IV. DISCUSSION

A. USING DAYTIME VNIR IMAGES TO DOWNSCALE NIGHTTIME LST

In the past, the explanatory variables used in daytime LST downscaling were constructed from images of VNIR bands, which were obtained in the daytime. However, for downscaling nighttime LST, the VNIR bands cannot form images at night. Moreover, in practice, due to the long revisit period of Landsat satellites and the influence of clouds, the date of formation of available VNIR images by remote sensors on Landsat satellites may be several days different from that of MODIS thermal infrared images. Therefore, only VNIR images taken in daytime (and most likely several days ago) can be used to construct explanatory variables for nighttime LST downscaling. Is that reasonable?

To answer this question, it is necessary to analyze the following two classic questions retrospectively. (1) How do spatial LST variations form? For the sake of simplification, only a case with clear sky, no wind, small spatial scale and urban surface is discussed here. As LST is the state variable of the SEB, the spatial variation of any component (including incoming shortwave radiation, reflected shortwave radiation, outgoing longwave radiation, incoming longwave radiation, latent heat flux, sensible heat flux and subsurface heat flux) in the SEB will lead to spatial variations of the LST, while spatial variations of the SEB components mainly depend on land surface characteristics, including albedo, emissivity, specific heat, density of soil or building materials, roughness length, thermal conductivity, soil moisture, vegetation type, and leaf area index. (2) What is the principle that allows VNIR-band images to be used as explanatory variables of LST spatial variations? DN values or their derived data (such as reflectivity and NDVI) of VNIR bands can directly or indirectly represent one or several of the land surface characteristics mentioned above, so a statistical correlation exists between them and the LST. Moreover, because these surface characteristics are basically stable over one or more days, the instantaneous information recorded in the VNIR bands can be used to represent the stable normality of the spatial variations of surface characteristics. For example, the spatial variations of vegetation quantities reflected by vegetation index images will not change from day to night and will not change significantly in a few days; therefore, it should not

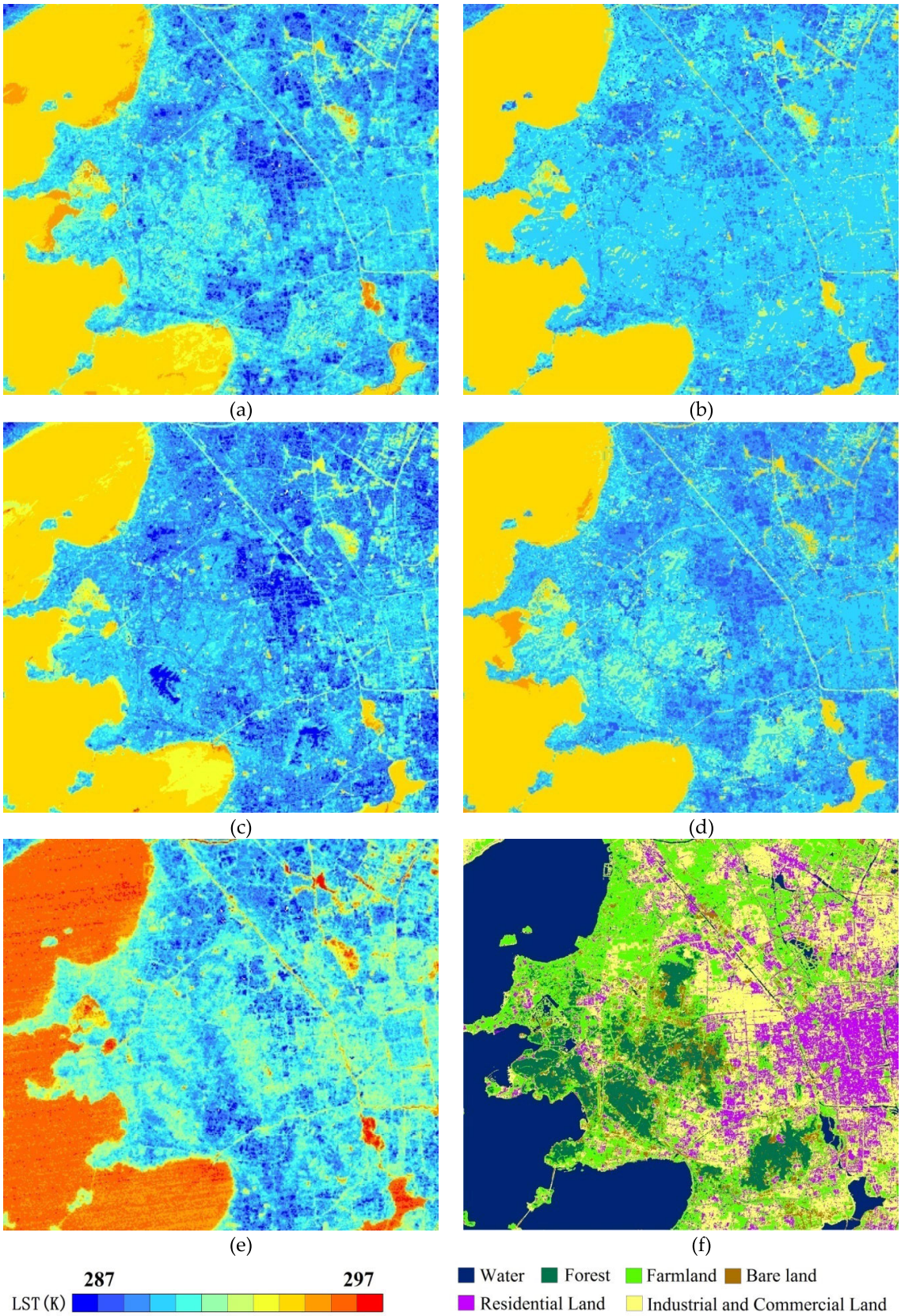

FIGURE 3. Downscaling results, validation image and land use and cover type (local). (a) Down_NLST$_1$; (b) Down_NLST$_2$; (c) Down_NLST$_3$; (d) Down_NLST$_4$; (e) Validation image (ASTER_NLST); (f) Land cover type.

be considered that the vegetation index image formed during daytime a few days ago is not suitable for representing the vegetation quantity tonight. This is the basic principle of statistical LST downscaling whether it is daytime or nighttime. Therefore, it is reasonable to use daytime VNIR images (and most likely obtained several days ago) to downscale nighttime LST.

In the study of Nichol [37], emissivity was employed as the only explanatory variable. Zhan *et al.* [1] also noted that other surface characteristics (such as NDVI and albedo) other than surface emissivity are not suitable for nighttime LST downscaling. However, due to heat storage in building interiors, vegetation canopies and deep soil, the spatial differentiation pattern of LST formed in the daytime will still be reflected at night. After sunset, the land surface produces different long-wave radiation due to different emissivities and temperatures; different subsurface heat fluxes due to different thermal conductivities, densities, and specific heat capacities; and different sensible heat fluxes due to different roughness lengths. The spatial variations of these processes lead to the further evolution of the spatial variability pattern of LST formed in daytime and thus form a new spatial variability pattern of LST. Therefore, when conducting nighttime LST downscaling, it is not sufficient to exclusively use emissivity as the explanatory variable. The above land surface characteristics should be reflected in the LST downscaling model as much as possible either directly or indirectly.

B. MECHANISM EXPLANATORY VARIABLE AND SPECTRAL EXPLANATORY VARIABLE

This study has shown that the downscaling results based on mechanism explanatory variables exhibit higher errors than those based on spectral explanatory variables. This finding indicates that, without adding external data, only combining and transforming spectral data (i.e., establishing the so-called mechanism explanatory variables) cannot improve the ability to interpret LST spatial variation.

A previous study has demonstrated that the information contained in spectral explanatory variables far exceeds a single remote sensing index, which can reflect various characteristics of land surface. With the support of machine learning algorithm, the high-dimensional feature space is automatically divided into many subspaces, and the specific relationship between LST and spectral explanatory variables is determined separately in each of them, thus avoiding the disadvantages of using higher-order polynomial function to simulate LST (e.g., over fitting and high sensitivity to sample noise) [28]. The results of this study support that view, and further analysis is provided below.

Although mechanism variables exhibit more explicit directivity than spectral variables (i.e., each mechanism variable is more inclined to represent certain specific environmental factor, for example, NDVI represents vegetation quantity), these variables could minimally represent other factors. In other words, a one-to-many relationship exists between a spectral variable and some environmental factors, whereas a one-to-one relationship exhibits between a mechanism variable and an environmental factor. The purpose of this study was to test whether it is more effective to construct explanatory variables through simple combination and transformation of spectral data without adding any exogenous data compared with directly using spectral data as explanatory variables. Limited by not adding exogenous data, the mechanism variables could neither reflect all environmental factors that will influence nighttime LST comprehensively and accurately nor have a one-to-many relationship like spectral variables. Therefore, downscaling results based on mechanism explanatory variables are inferior to those based on spectral variables.

The above findings suggest that spectral variables should be used directly in the actual operation of nighttime LST downscaling. Since the process of producing various remote sensing indexes (i.e., the mechanism explanatory variable referred to in this paper) is omitted, this method can be easily developed as an automatic data processing program.

C. SOURCE OF ERROR

The downscaling results of this study have certain errors, which are believed caused by the following: (1) self-errors of models, which refer to errors caused by poor explanation to target variable (i.e., LST) caused by inaccurate or (and) incomprehensive explanatory variables or the failure of the established statistical model to describe the complicated relationship between explanatory variables and target variable. Specifically, it can be further divided into two types according to sources. First, the MODIS_NLST was obtained on October 1st, 2015, while the original Landsat 8 OLI/TIRS data for constructing explanatory variable images were obtained on October 13th, 2015. The later were used to represent the environmental features on previous date (October 1st, 2015). However, a 12-day difference was noted between these two dates, during which the environmental features would change slightly. Second, pixels in MODIS_NLST images with large errors were eliminated by QA (2 K as threshold), but the remaining pixel values still had errors. The threshold of removing low quality pixels cannot be stricter because a standard that is too strict will lead to an insufficient number of samples. Self-errors of models could be transmitted to final results. (2) Scale-conversion errors, which refer to the errors occur when the models built at coarse resolution were applied at fine resolution. In this study, the errors of final results are significantly larger than the self-errors of models (e.g., the self RMSE of the MARS model based on the spectral explanatory variables is 0.631 K, whereas the RMSE of the final result based on this model is 1.758 K), indicating that the scale-conversion errors occurred when the 1000-m scale models are used for the 30-m resolution explanatory variables.

D. POTENTIAL USE OF THIS METHOD

This method provides a possibility for researchers to obtain fine-resolution nighttime LST images. The images are

important basic data in the fields of meteorology, ecology, and environment.

One example of such image application is urban air pollution research. At present, air pollution has become one of the most obvious environmental problems in large cities around the globe. Air pollution is often caused by many factors, and radiation inversion is considered an important factor [58], [59]. Radiation inversion refers to a relatively cool layer of air, which is usually adjacent to some underlying surfaces cooled by a net loss of radiation. Inversion of temperature causes atmospheric stability that restricts upward and downward air movements such that pollutants may remain suspended in a low air layer over a long period and has serious impacts on the health of the citizens [60]. Due to the different thermal properties of lands with different use and cover types, the formation processes and strengths of radiation inversions above different land surfaces are different. The method proposed in this paper provides the possibility to analyze the relationship between nighttime radiation inversion and land use and cover types on a fine spatial scale. Based on the fine-resolution night LST images generated by this method, it is shown that the surface temperatures of factories and warehouses are significantly lower than those of other objects. Therefore, we speculate that radiation inversions are more likely to form over large areas of continuously distributed factories and warehouses, thus enhancing air pollution in these areas. In recent years, under the background of the rapid development of the manufacturing industry, the total area of factories and warehouses in many Chinese cities has been growing rapidly and now has become a major land type. If this large-scale land use and cover change changes the surface energy budget, which leads to the aggravation of air pollution, it will be a very noteworthy problem. To confirm this inference, it is necessary to perform a comprehensive study of the thermal properties and energy budgets of land surfaces as well as the atmospheric stability of the atmospheric boundary layer in areas with concentrated distributions of factories and warehouses. The fine-resolution nighttime LST images produced by this method will be an important data source for that research.

Another example of the potential application of fine-resolution night LST images is urban thermal environment assessment and planning. Urban climate has a profound impact on many aspects of people's life and urban operation. LST is an important aspect of urban climate that directly affects the physical health and outdoor activity intensity of citizens, and indirectly affects their mental health, life rhythm and energy consumption of the city. The spatial distribution pattern of LST has become an important factor in urban environmental assessment and planning. Compared with the daytime, the surface temperature at night has special environmental significance: (1) for many people in cities, night is the main period of outdoor leisure activities, and the influence of outdoor environmental comfort on people's choice of outdoor activities is more obvious at night; (2) in the daytime, human's cold and hot feelings about the environment depend on the solar radiation, long-wave radiation from the surrounding environment and the atmosphere, the heat conduction and convection between the body surface and the air. After sunset, given the influence of solar radiation disappears, the influence of long-wave radiation becomes more important. The method proposed in this study provides fine-resolution LST images, which can reflect the spatial distribution pattern of long-wave radiation in detail and provide important data sources for future environmental assessment planning for thermal comfort.

V. CONCLUSION

Downscaling has always been an important method for obtaining fine-resolution LST images, but most of the previous downscaling methods were proposed for daytime LST images. In this study, using 1000-m resolution nighttime MODIS LST products and 30-m resolution daytime Landsat 8 images as experimental materials, the performance of multivariable statistical method in nighttime LST downscaling was evaluated. Verification using ASTER LST image shows that the downscaling errors are acceptable (the MAE values vary from 1.475 to 1.761 K). Compared with the previous studies focused on daytime LST downscaling, the accuracy of nighttime downscaling results obtained in this study is satisfactory. The downscaled images clearly reveal the spatial differentiation pattern of nighttime LST in the study area and can provide the possibility to analyze the relationships of LST with land use and cover type on a fine spatial scale.

This study indicates that it is reliable and reasonable to downscale nighttime LST images by using the VNIR images obtained in the daytime (and most likely obtained several days ago). The study also indicated that the spectral explanatory variables outperform mechanism explanatory variables for nighttime LST downscaling; thus, the method can be more easily developed into an automated image processing program.

This method only requires several satellite remote sensing images that are easy to obtain for ordinary users, so it is simple and thus feasible. It is believed that this method has important application value in many studies and practices of urban meteorology, ecology, environment and other fields.

ACKNOWLEDGMENT

The authors would like to thank the United States Geological Survey for providing the Landsat 8 and ASTER data products. They would also like to thank the Level-1 and Atmosphere Archive & Distribution System Distributed Active Archive Center for providing Terra MODIS data.

REFERENCES

[1] W. Zhan, Y. Chen, J. Zhou, J. Wang, W. Liu, J. Voogt, X. Zhu, J. Quan, and J. Li, "Disaggregation of remotely sensed land surface temperature: Literature survey, taxonomy, issues, and caveats," *Remote Sens. Environ.*, vol. 131, pp. 119–139, Apr. 2013.

[2] X. Yu, X. Guo, and Z. Wu, "Land surface temperature retrieval from landsat 8 TIRS—Comparison between radiative transfer equation-based method, split window algorithm and single channel method," *Remote Sens.*, vol. 6, no. 10, pp. 9829–9852, Oct. 2014.

[3] Y. Hu and G. Jia, "Influence of land use change on urban heat island derived from multi-sensor data," *Int. J. Climatol.*, vol. 30, no. 9, pp. 1382–1395, Jul. 2010.

[4] A. Dominguez, J. Kleissl, J. C. Luvall, and D. L. Rickman, "High-resolution urban thermal sharpener (HUTS)," *Remote Sens. Environ.*, vol. 115, no. 7, pp. 1772–1780, Jul. 2011.

[5] B. Bechtel, K. Zakšek, and G. Hoshyaripour, "Downscaling land surface temperature in an urban area: A case study for hamburg, germany," *Remote Sens.*, vol. 4, no. 10, pp. 3184–3200, Oct. 2012.

[6] V. Barraza, F. Grings, M. Franco, V. Douna, D. Entekhabi, N. Restrepo-Coupe, A. Huete, M. Gassmann, and E. Roitberg, "Estimation of latent heat flux using satellite land surface temperature and a variational data assimilation scheme over a eucalypt forest savanna in northern Australia," *Agricult. Forest Meteorol.*, vol. 268, pp. 341–353, Apr. 2019.

[7] M. Anderson, J. Norman, W. Kustas, R. Houborg, P. Starks, and N. Agam, "A thermal-based remote sensing technique for routine mapping of land-surface carbon, water and energy fluxes from field to regional scales," *Remote Sens. Environ.*, vol. 112, no. 12, pp. 4227–4241, Dec. 2008.

[8] C. Huang, W. Chen, Y. Li, H. Shen, and X. Li, "Assimilating multi-source data into land surface model to simultaneously improve estimations of soil moisture, soil temperature, and surface turbulent fluxes in irrigated fields," *Agricult. Forest Meteorol.*, vols. 230–231, pp. 142–156, Dec. 2016.

[9] N. T. Son, C. F. Chen, C. R. Chen, L. Y. Chang, and V. Q. Minh, "Monitoring agricultural drought in the lower mekong basin using MODIS NDVI and land surface temperature data," *Int. J. Appl. Earth Observ. Geoinf.*, vol. 18, pp. 417–427, Aug. 2012.

[10] M. E. Holzman, R. Rivas, and M. C. Piccolo, "Estimating soil moisture and the relationship with crop yield using surface temperature and vegetation index," *Int. J. Appl. Earth Observ. Geoinf.*, vol. 28, pp. 181–192, May 2014.

[11] L. Zhang, W. Jiao, H. Zhang, C. Huang, and Q. Tong, "Studying drought phenomena in the continental united states in 2011 and 2012 using various drought indices," *Remote Sens. Environ.*, vol. 190, pp. 96–106, Mar. 2017.

[12] M. Minacapilli, S. Consoli, D. Vanella, G. Ciraolo, and A. Motisi, "A time domain triangle method approach to estimate actual evapotranspiration: Application in a mediterranean region using MODIS and MSG-SEVIRI products," *Remote Sens. Environ.*, vol. 174, pp. 10–23, Mar. 2016.

[13] G. B. Senay, M. Friedrichs, R. K. Singh, and N. M. Velpuri, "Evaluating landsat 8 evapotranspiration for water use mapping in the colorado river basin," *Remote Sens. Environ.*, vol. 185, pp. 171–185, Nov. 2016.

[14] K. Knipper, T. Hogue, R. Scott, and K. Franz, "Evapotranspiration estimates derived using multi-platform remote sensing in a semiarid region," *Remote Sens.*, vol. 9, no. 3, p. 184, Feb. 2017.

[15] B. Dousset, F. Gourmelon, K. Laaidi, A. Zeghnoun, E. Giraudet, P. Bretin, E. Mauri, and S. Vandentorren, "Satellite monitoring of summer heat waves in the Paris metropolitan area," *Int. J. Climatol.*, vol. 31, no. 2, pp. 313–323, Feb. 2011.

[16] J. Azevedo, L. Chapman, and C. Muller, "Quantifying the daytime and night-time urban heat island in Birmingham, UK: A comparison of satellite derived land surface temperature and high resolution air temperature observations," *Remote Sens.*, vol. 8, no. 2, p. 153, Feb. 2016.

[17] P. Sismanidis, I. Keramitsoglou, and C. T. Kiranoudis, "Evaluating the operational retrieval and downscaling of urban land surface temperatures," *IEEE Geosci. Remote Sens. Lett.*, vol. 12, no. 6, pp. 1312–1316, Jun. 2015.

[18] R. Bala, R. Prasad, and V. Pratap Yadav, "Disaggregation of modis land surface temperature in urban areas using improved thermal sharpening techniques," *Adv. Space Res.*, vol. 64, no. 3, pp. 591–602, Aug. 2019.

[19] H. Ebrahimy and M. Azadbakht, "Downscaling MODIS land surface temperature over a heterogeneous area: An investigation of machine learning techniques, feature selection, and impacts of mixed pixels," *Comput. Geosci.*, vol. 124, pp. 93–102, Mar. 2019.

[20] D. Liu and X. Zhu, "An enhanced physical method for downscaling thermal infrared radiance," *IEEE Geosci. Remote Sens. Lett.*, vol. 9, no. 4, pp. 690–694, Jul. 2012.

[21] E. Barbierato, I. Bernetti, I. Capecchi, and C. Saragosa, "Quantifying the impact of trees on land surface temperature: A downscaling algorithm at city-scale," *Eur. J. Remote Sens.*, vol. 52, no. 4, pp. 74–83, Dec. 2019.

[22] Q. Weng, P. Fu, and F. Gao, "Generating daily land surface Temperature at Landsat resolution by fusing Landsat and MODIS data," *Remote Sens. Environ.*, vol. 145, pp. 55–67, Apr. 2014.

[23] P. Wu, H. Shen, L. Zhang, and F.-M. Göttsche, "Integrated fusion of multi-scale polar-orbiting and geostationary satellite observations for the mapping of high spatial and temporal resolution land surface temperature," *Remote Sens. Environ.*, vol. 156, pp. 169–181, Jan. 2015.

[24] J. Wang, O. Schmitz, M. Lu, and D. Karssenberg, "Thermal unmixing based downscaling for fine resolution diurnal land surface temperature analysis," *ISPRS J. Photogramm. Remote Sens.*, vol. 161, pp. 76–89, Mar. 2020.

[25] W. P. Kustas, J. M. Norman, M. C. Anderson, and A. N. French, "Estimating subpixel surface temperatures and energy fluxes from the vegetation index–radiometric temperature relationship," *Remote Sens. Environ.*, vol. 85, no. 4, pp. 429–440, Jun. 2003.

[26] N. Agam, W. P. Kustas, M. C. Anderson, F. Li, and C. M. U. Neale, "A vegetation index based technique for spatial sharpening of thermal imagery," *Remote Sens. Environ.*, vol. 107, no. 4, pp. 545–558, Apr. 2007.

[27] W. Essa, B. Verbeiren, J. van der Kwast, T. Van De Voorde, and O. Batelaan, "Evaluation of the DisTrad thermal sharpening methodology for urban areas," *Int. J. Appl. Earth Observ. Geoinf.*, vol. 19, pp. 163–172, Oct. 2012.

[28] F. Gao, W. Kustas, and M. Anderson, "A data mining approach for sharpening thermal satellite imagery over land," *Remote Sens.*, vol. 4, no. 11, pp. 3287–3319, Oct. 2012.

[29] A. Ghosh and P. K. Joshi, "Hyperspectral imagery for disaggregation of land surface temperature with selected regression algorithms over different land use land cover scenes," *ISPRS J. Photogramm. Remote Sens.*, vol. 96, pp. 76–93, Oct. 2014.

[30] G. Yang, R. Pu, W. Huang, J. Wang, and C. Zhao, "A novel method to estimate subpixel temperature by fusing solar-reflective and thermal-infrared remote-sensing data with an artificial neural network," *IEEE Trans. Geosci. Remote Sens.*, vol. 48, no. 4, pp. 2170–2178, Apr. 2010.

[31] Q. Weng and P. Fu, "Modeling diurnal land temperature cycles over Los Angeles using downscaled GOES imagery," *ISPRS J. Photogramm. Remote Sens.*, vol. 97, pp. 78–88, Nov. 2014.

[32] Y. Yang, C. Cao, X. Pan, X. Li, and X. Zhu, "Downscaling land surface temperature in an arid area by using multiple remote sensing indices with random forest regression," *Remote Sens.*, vol. 9, no. 8, pp. 789–807, Jul. 2017.

[33] X. Pan, X. Zhu, Y. Yang, C. Cao, X. Zhang, and L. Shan, "Applicability of downscaling land surface temperature by using normalized difference sand index," *Sci. Rep.*, vol. 8, no. 1, pp. 9530–9544, Jun. 2018.

[34] J. W. Wang, W. T. L. Chow, and Y.-C. Wang, "A global regression method for thermal sharpening of urban land surface temperatures from MODIS and Landsat," *Int. J. Remote Sens.*, vol. 41, no. 8, pp. 2986–3009, Apr. 2020.

[35] P. Qi, S. Hu, H. Zhang, and G. Guo, "Sharpening method of satellite thermal image based on the geographical statistical model," *J. Appl. Remote Sens.*, vol. 10, no. 2, May 2016, Art. no. 025013.

[36] C. Hutengs and M. Vohland, "Downscaling land surface temperatures at regional scales with random forest regression," *Remote Sens. Environ.*, vol. 178, pp. 127–141, Jun. 2016.

[37] J. Nichol, "An emissivity modulation method for spatial enhancement of thermal satellite images in urban heat island analysis," *Photogramm. Eng. Remote Sens.*, vol. 75, no. 5, pp. 547–556, May 2009.

[38] F. Wang, Z. Qin, W. Li, C. Song, A. Karnieli, and S. Zhao, "An efficient approach for pixel decomposition to increase the spatial resolution of land surface temperature images from MODIS thermal infrared band data," *Sensors*, vol. 15, no. 1, pp. 304–330, Dec. 2014.

[39] X. Zhang, H. Zhao, and J. Yang, "Spatial downscaling of land surface temperature in combination with TVDI and elevation," *Int. J. Remote Sens.*, vol. 40, nos. 5–6, pp. 1875–1886, Mar. 2019.

[40] T. R. Oke, *Boundary Layer Climates*, 2nd ed. London, U.K.: Routledge, 1987, pp. 110–157.

[41] S. M. Bateni and D. Entekhabi, "Relative efficiency of land surface energy balance components," *Water Resour. Res.*, vol. 48, no. 4, pp. 1–8, Apr. 2012.

[42] R. B. Stull, *An Introduction to Boundary Layer Meteorology*. Dordrecht, The Netherlands: Kluwer, 1988, pp. 251–294.

[43] W. G. M. Bastiaanssen, "SEBAL-based sensible and latent heat fluxes in the irrigated Gediz Basin, Turkey," *J. Hydrol.*, vol. 229, nos. 1–2, pp. 87–100, Mar. 2000.

[44] *Landsat 8 (L8) Data Users Handbook*. United States Geological Survey, Sioux Falls, SD, USA. Accessed: Mar. 29, 2016. [Online]. Available: https://www.usgs.gov/media/files/landsat-8-data-users-handbook

[45] X. X. Zhang, P. F. Wu, and B. Chen, "Relationship between vegetation greenness and urban heat island effect in Beijing City of China," *Procedia Environ. Sci.*, vol. 2, pp. 1438–1450, Jan. 2010.
[46] S. M. Jaber, "Landsat-based vegetation abundance and surface temperature for surface urban heat island studies: The tale of greater amman municipality," *Ann. GIS*, vol. 24, no. 3, pp. 195–208, May 2018.
[47] S. Liang, "Narrowband to broadband conversions of land surface albedo I: Algorithms," *Remote Sens. Environ.*, vol. 76, pp. 213–238, May 2001.
[48] H. Xu, "Retrieval of the reflectance and land surface temperature of the newly-launched Landsat 8 satellite," *Chin. J. Geophys.*, vol. 58, no. 3, pp. 741–747, Mar. 2015.
[49] P. S. Chavez, "Image-based atmospheric corrections-revisited and improved," *Photogramm. Eng. Remote Sens.*, vol. 62, no. 9, pp. 1025–1036, 1996.
[50] H. Xu, "Modification of normalised difference water index (NDWI) to enhance open water features in remotely sensed imagery," *Int. J. Remote Sens.*, vol. 27, no. 14, pp. 3025–3033, Jul. 2006.
[51] I. Sandholt, K. Rasmussen, and J. Andersen, "A simple interpretation of the surface temperature/vegetation index space for assessment of surface moisture status," *Remote Sens. Environ.*, vol. 79, nos. 2–3, pp. 213–224, Feb. 2002.
[52] ArcGIS Resource Center. *How Zonal Statistics Works*. Accessed: Jan. 21, 2018. [Online]. Available: http://help.arcgis.com/en/arcgisdesktop/10.0/help/index.html#//009z000000wt000000.htm
[53] J. H. Friedman, "Multivariate adaptive regression splines," *Annu. Statist.*, vol. 19, no. 1, pp. 1–67, Mar. 1991.
[54] D. Steinberg and M. Golovnya, "CART 6.0 user's guide," Salford Syst. Co., San Diego, CA, USA, 2006. [Online]. Available: http://dist.salford-systems.com/CART6/CART6.pdf
[55] C. Jeganathan, N. A. S. Hamm, S. Mukherjee, P. M. Atkinson, P. L. N. Raju, and V. K. Dadhwal, "Evaluating a thermal image sharpening model over a mixed agricultural landscape in India," *Int. J. Appl. Earth Observ. Geoinf.*, vol. 13, no. 2, pp. 178–191, Apr. 2011.
[56] S. Mukherjee, P. Kumar Joshi, and R. D. Garg, "Regression-Kriging technique to downscale satellite-derived land surface temperature in heterogeneous agricultural landscape," *IEEE J. Sel. Topics Appl. Earth Observ. Remote Sens.*, vol. 8, no. 3, pp. 1245–1250, Mar. 2015.
[57] J. R. Jensen, *Remote Sensing of the Environment: An Earth Resource Perspective*, 2nd ed. Upper Saddle River, NJ, USA: Prentice-Hall, 2007, pp. 525–590.
[58] J. Khodakarami and P. Ghobadi, "Urban pollution and solar radiation impacts," *Renew. Sustain. Energy Rev.*, vol. 57, pp. 965–976, May 2016.
[59] J. Zhong, X. Zhang, Y. Wang, J. Sun, Y. Zhang, J. Wang, K. Tan, X. Shen, H. Che, L. Zhang, Z. Zhang, X. Qi, H. Zhao, S. Ren, and Y. Li, "Relative contributions of boundary-layer meteorological factors to the explosive growth of PM2.5 during the red-alert heavy pollution episodes in Beijing in December 2016," *J. Meteorol. Res.*, vol. 31, no. 5, pp. 809–819, Oct. 2017.
[60] E. Malek, T. Davis, R. S. Martin, and P. J. Silva, "Meteorological and environmental aspects of one of the worst national air pollution episodes (January, 2004) in Logan, Cache Valley, Utah, USA," *Atmos. Res.*, vol. 79, no. 2, pp. 108–122, Feb. 2006.

PENGCHENG QI was born in Yishui, Shandong, China, in 1978. He received the M.S. degree from Northwest Normal University, China, in 2005, and the Ph.D. degree from Lanzhou University, China, in 2009. In 2010, he joined Nanyang Normal University, where he is currently an Associate Professor and a Researcher with the Collaborative Innovation Center of Water Security for Water Source Region of Mid-Line of South-to-North Diversion Project of Henan Province. He has authored over 30 research articles. His research interests include remote sensing digital image processing and thermal infrared remote sensing. His research has been sponsored by the National Natural Science Foundation of China. In 2013, he was elected to be Wolong Scholar of Nanyang Normal University.

YAN CUI was born in Tancheng, Shandong, China, in 1978. She received the Ph.D. degree from the Institute of Environment and Engineering in Cold and Arid Regions, Chinese Academy of Sciences, China, in 2009. She is currently a Member with the Collaborative Innovation Center of Water Security for Water Source Region of Mid-Line of South-to-North Diversion Project of Henan Province, Nanyang Normal University. Her research interests include environmental ecology and ecological hydrology.

HAIJUN ZHANG was born in Luanping, Hebei, China, in 1978. He received the B.S. degree in geographic information systems and the M.S. degree in cartography and geographic information engineering from Chang'an University, China. He is currently a member with the Collaborative Innovation Center of Water Security for Water Source Region of Mid-Line of South-to-North Diversion Project of Henan Province, Nanyang Normal University. He has authored over 20 research articles. His research interests include the integration of remote sensing and GIS in addressing environmental issues.

SHIXIONG HU received the Ph.D. degree in physical geography from the State University of New York at Buffalo, in 2004. He is currently a Professor of geography with the Department of History and Geography, East Stroudsburg University of Pennsylvania. He has authored over 50 research articles. His research interests include water resources management and GIS/RS applications. His research has been sponsored by the National Natural Science Foundation of China, NASA, the United States Fish and Wildlife Service, and the Pennsylvania Department of Conservation and Natural Resources. He is a member of the American Geophysical Union (AGU), the international Association of Hydrological Sciences (IAHS), the American Association of Geographers (AAG), the International Association for Hydro-Environment Engineering and Research (IAHR), and the Chinese Professional in Geographic Information Systems (CPGIS). He received CPGIS Annual Service Excellence Individual Awards in 2012 and 2013. He has served as an editor in various international conferences and journals.

LUNGUANG YAO was born in Shaoyang, Hunan, China, in 1974. He received the Ph.D. degree from Wuhan University, in 2004. He is currently the Head Researcher with the Collaborative Innovation Center of Water Security for Water Source Region of Mid-Line of South-to-North Diversion Project of Henan Province, Nanyang Normal University. He has authored over 60 research articles. His research interests include environmental ecology and environmental monitoring.

LARRY BAILIAN LI was born in Jingmen, Hubei, China, in 1962. He received the Ph.D. degree in ecology from Texas A&M University. He is currently a Professor of ecology with the University of California–Riverside. He has published more than 250 refereed journal articles, 30 book chapters and proceedings articles, and 11 books or edited special issues. His research interests include mathematical, statistical, and computational modeling applications in ecological and environmental studies. He is the Founding Editor-in-Chief of two international journals: *Ecological Complexity* (Elsevier) and the *Journal of Arid Land* (Springer Nature). He was elected to be an Honorary Professor of the Scientific Council of Russian Academy of Sciences in 2005 and the American Association for the Advancement of Science Fellow in 2006. He received the Prigogine Gold Medal in 2015.